# Phase Behaviors and Molecular and Supramolecular Structural Identifications of a Liquid Crystalline Second Generation Monodendron

Zhen Liu,[†] Lei Zhu,[†] Wensheng Zhou,[†] Stephen Z. D. Cheng,*[,†] Vigil Percec,[‡] and Goran Ungar[§]

*Murice Morton Institute and Department of Polymer Science, The University of Akron, Akron, Ohio 44325-3909; Department of Chemistry, University of Pennsylvania, Philadelphia, Pennsylvania 19104-6323; and Department of Engineering Materials, University of Sheffield, Sheffield S1 3JD, UK*

*Received December 20, 2001. Revised Manuscript Received March 26, 2002*

A second generation monodendron (abbreviated as $G_2NB$) based on the $AB_2$ mesogenic monomer, 13-hydroxy-1-(4-hydroxyphenyl)-2-(4-hydroxy-4″-*p*-terphenylyl)tridecane building blocks, exhibits multiple mesophase transformations with varying temperatures. On the basis of thermal transition behaviors studied by differential scanning calorimetry, structural analyses carried out by wide-angle and small-angle X-ray scatterings and electron diffraction experiments, and morphologies observed in polarized light microscope, the equilibrium phase transition sequence and phase structures have been identified. From the glass transition temperature at 28 °C, the most ordered phase is a highly ordered liquid crystalline (LC) smectic B ($S_h^B$) phase. This phase is defined on the basis of the relationship between the LC mesogenic orientation direction and the layer normal. Within the layers, a molecular lateral hexagonal packing exists. It is followed by a low ordered LC smectic C ($S_C$) phase appeared in a narrow temperature range of ∼2 °C and quickly entered a nematic phase. At a high temperature of 92 °C, $G_2NB$ reaches the isotropic melt. An interesting observation is that the layer spacing of these $S_h^B$ and $S_C$ phases are much larger than the chemical repeat unit of the LC monomer; rather, it is a representative of the whole size of the $G_2NB$ monodendron. Therefore, the $S_h^B$ phase is a combined supramolecular layer structure and a lateral molecular hexagonal packing, while the $S_C$ phase is a pure supramolecular phase. A surprising finding is that the supramolecular $S_C$ phase formation possesses a stronger cooling rate dependence than that of the $S_h^B$ phase formation. This provides an opportunity to control the appearance of the $S_C$ phase formation by only varying the cooling rate. Possible packing structural model and formation mechanisms of this phenomenon are discussed.

## Introduction

One of the molecular self-assemblies is to form highly organized liquid crystalline (LC) aggregates. The most suitable architectures for the formation of thermotropic LC phases are rod- or disklike molecules.[1] However, the typical dendrimers and hyperbranched polymers possess spheroidal or ellipsoidal shapes.[2−7] The formation of LC phases in dendrimers and hyperbranched polymers had been difficult. Recently, two general approaches to design and construct the dendritic skeletons which possess LC phases have been proposed.[8−13] The first approach is to utilize building blocks to self-assemble supramolecular LC phase, such as an attachment of a semirigid dendritic wedge to an ether chain or crown ether which functions as an endo receptor. Although monodendron itself does not possess typical mesogenic groups, it can undergo self-assembly to generate a tubular or spherical architecture that constructs a hexagonal columnar or cubic supramolecular LC phases. Examples include 3,4,5-tris(4-alkyl-1-oxy)benzyloxybenzoate to form tapered monodendrons, which form the columnar phase, while 3,4,5-tris[3′,4′,5′-tris(alkyl-1-oxy)-benzyloxy]benzoate exhibits a conical shape, which

* To whom correspondence should be addressed. E-mail: cheng@polymer.uakron.edu.
[†] The University of Akron.
[‡] University of Pennsylvania.
[§] University of Sheffield.

(1) de Gennes, P. G. *The Physics of Liquid Crystals*; Oxford University Press: Oxford, 1974; 2nd ed., 1993.
(2) Wooley, K. L.; Hawker, C. J.; Fréchet, J. M. J. *J. Am. Chem. Soc.* **1991**, *113*, 4252.
(3) Wooley, K. L.; Hawker, C. J.; Fréchet, J. M. J. *J. Chem. Soc., Perkin Trans. 1* **1991**, 1059.
(4) Kim, Y. H.; Webster, O. W. *J. Am. Chem. Soc.* **1990**, *112*, 3687.
(5) Fréchet, J. M. J. *Science* **1994**, *263*, 1710.
(6) Tomalia, D. A.; Durst, H. D. *Top. Curr. Chem.* **1993**, *165*, 193.
(7) Tomalia, D. A. *Sci. Am.* **1995** (May), 62.
(8) Balagurusamy, V. S. K.; Ungar, G.; Percec, V.; Johansson, G. *J. Am. Chem. Soc.* **1997**, *119*, 1539.
(9) Percec, V.; Ahn C.-H.; Ungar, G.; Yeardley, D. J. P.; Moller, M.; Sheiko, S. S. *Nature (London)* **1998**, *391*, 161.
(10) Percec, V.; Heck, J. A.; Tomazos, D.; Falkenberg, F.; Blackwell, H.; Ungar, G. *J. Chem. Soc., Perkin Trans. 1* **1993**, 2799.
(11) Percec, V.; Heck, J. A.; Tomazos, D.; Ungar, G. *J. Chem. Soc., Perkin Trans. 2* **1993**, 2381.
(12) Percec, V.; Chu, P. *Proc. Am. Chem. Soc., Div. Polym. Mater., Sci. Eng.* **1995**, *73*, 125.
(13) Hudson, S. D.; Jung, H.-T.; Percec, V.; Cho, W.-D.; Johansson, G.; Ungar, G.; Balagurusamy, V. S. K. *Science* **1997**, *278*, 449.

10.1021/cm0117228 CCC: $22.00 
Published on Web 04/26/2002

constructs spheres to form the cubic assembly. These supramolecular self-assemblies presumably result from segregation of the aromatic and aliphatic moieties.[8,9] It has been demonstrated that size and shape of a supramolecular LC dendrimer are determined by the solid angle (i.e., the planar angle) of the monodendrons. In general, with increasing generation numbers the solid angle of the flat tapered and conical monodendron increases until each molecule becomes a single sphere.

The second approach is based on the mesogenic character of $AB_2$ monomers to build a dendrimer or a hyperbranched polymer that displays thermotropic molecular LC phases.[14−18] One of the examples is 13-hydroxy-1-(4-hydroxyphenyl)-2-(4-hydroxy-4″-*p*-terphylyl)-tridecane, which is a building block of the monodendrons in different generations.[16] The chemical structure of $AB_2$ is

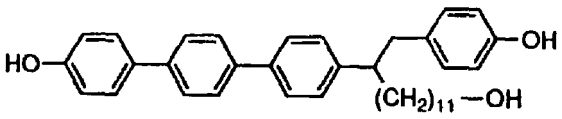


This rodlike $AB_2$ monomer possesses a carbon linkage at the $(CH_2)_{11}$ position which exhibits conformational flexibility. The bond rotation at this flexible carbon linkage leads to different conformational isomers, of which the stable states are anti and gauche. The anti isomer has an extended conformation and may result in mesogens aligning almost parallel to each other, whereas the gauche isomer, similar to a kinked unit, is associated with reductions of the transition temperatures and increases in the solubility. Some pure dendritic compounds have also been synthesized. Mono- and tridendrons up to the fourth generation have been prepared with 10-undecenyl groups on the periphery using iterative convergent strategy. The structure and phase characterization of these dendrimers show the existence of nematic (N) and smectic (S) phases.[16] Recently, several series of carbosilane-based LC dendrimers up to the fifth generation have also been synthesized by introducing cyanobiphenyl, methoxyphenyl benzoate, and cholesteryl groups as terminal groups.[19,20] Ferrocene-containing LC dendrimers[21] and ferroelectric dendritic LC polymers[22] have also been reported.

In this publication, we concentrate our attention on detailed structural identifications and phase transformations of a second generation monodendron having 13-hydroxy-1-(4-hydroxyphenyl)-2-(4-hydroxy-4″-*p*-terphylyl)-tridecane as building blocks. The chemical structure of this $G_2NB$ is

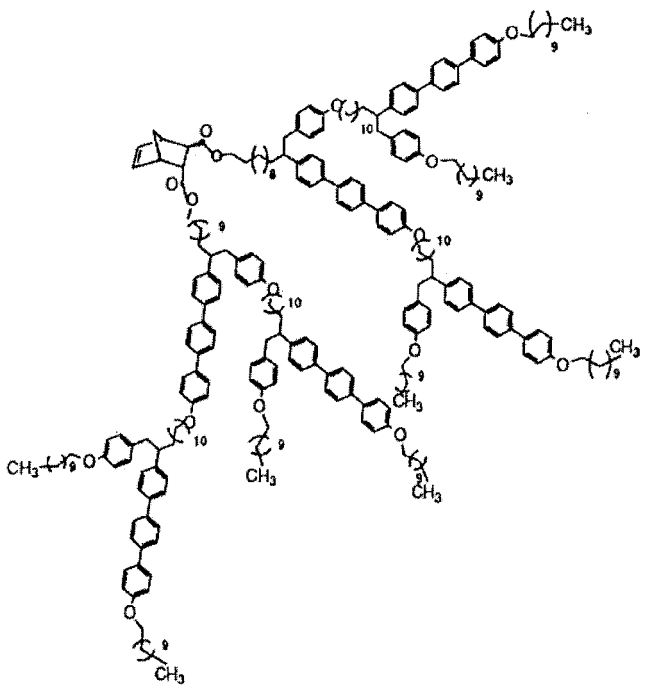

Three different LC phases can be formed in this monodendron based on experimental observations obtained from combined structural and morphological characterizations. In particular, a correlation between the molecular and supramolecular structures in different length scales is established. This may be directly linked to the change of phase transition behaviors in this monodendron.

## Experimental Section

**Materials.** A second generation monodendron was synthesized on the basis of the conformationally flexible $AB_2$ mesogenic monomer, 13-hydroxy-1-(4-hydroxyphenyl)-2-(4-hydroxy-4″-*p*-terphenylyl)tridecane building block, through a divergent strategy. The detailed synthetic route has been published elsewhere.[15]

**Experiments and Equipment.** Differential scanning calorimetry (DSC) experiments were performed on a Perkin-Elmer DSC-7 equipped with a cooling apparatus to study the thermal transition behaviors of $G_2NB$. The temperature and heat flow were calibrated using standard materials (indium and tin) at different cooling and heating rates between 1 and 40 °C/min under a dry nitrogen atmosphere. Different heating and cooling rates were used to examine the phase stability and the reversibility of the phase transitions. The cooling experiment was always first recorded in order to eliminate the thermal history and then followed by a heating scan at a heating rate equal to the previous cooling rate. The lower limit temperature in the experiments is below the glass transition temperature ($T_g$ = 28 °C). The onset transition temperatures were employed for both cooling (at low-temperature side) and heating (at high-temperature side) scans.

One-dimensional (1D) wide-angle X-ray diffraction (WAXD) powder experiments were performed with a Rigaku 12 kW rotating anode generator (Cu K$\alpha$, $\lambda$ = 0.154 nm) equipped with a Geigerflex D/max-RB diffractometer (radius of 185 mm). The X-ray beam was line-focused and monochromatized using a graphite crystal. The reflection peak positions and widths were calibrated with silicon crystals of known crystal size in the high-angle region ($2\theta > 15°$) and silver behenate for the low-angle region ($2\theta < 15°$). A hot stage coupled with the diffrac-

(14) Bauer, S.; Fischer, H.; Ringsdorf, H. *Angew. Chem., Int. Ed. Engl.* **1993**, *32*, 1589.
(15) Percec, V.; Chu, P.; Kawasumi, M. *Macromolecules* **1994**, *27*, 4441.
(16) Percec, V.; Chu, P.; Ungar, G.; Zhou, J. *J. Am. Chem. Soc.* **1995**, *117*, 11441.
(17) Li, J. F.; Crandall, K. A.; Chu, P. W.; Percec, V.; Petschek, R. G.; Rosenblatt, C. *Macromolecules* **1996**, *29*, 7813.
(18) Percec, V.; Chu, P.; Kawasumi, M. *Macromolecules* **1994**, *27*, 4441.
(19) Ponomarenko, S. A.; Rebrov, E. A.; Bobrovsky, A. Y.; Boiko, N. I.; Muzafarov, A. M.; Shibaev, V. P. *Liq. Cryst.* **1996**, *21*, 1.
(20) Lorenz, K.; Hotler, D.; Stuhn, B.; Mulhaupt, R.; Frey, H. A. *Adv. Mater.* **1996**, *8*, 414.
(21) Dardel, B.; Deschenaux, R.; Even, M.; Serrano, E. *Macromolecules* **1999**, *32*, 5193.
(22) Busson, P.; Ihre, H.; Hult, A. *J. Am. Chem. Soc.* **1998**, *120*, 9070.

tometer was used to study the phase transitions at heating and cooling rates between 1 and 10 °C/min (the fastest controllable cooling rate in the WAXD). The temperature deviation was controlled within ±0.5 °C. Samples with a thickness of ~0.1 mm were mounted on an aluminum sheet and scanned in a $2\theta$ angle range between 1.5° and 35°. Background scattering of the aluminum sheet was recorded and subtracted from the sample WAXD patterns. 1D small-angle X-ray scattering (SAXS) experiments at different temperatures were carried out at the synchrotron beamline X27C at Brookhaven National Laboratory. The wavelength of the X-ray beam was 0.1307 nm. An European Molecular Biology Laboratory positional sensitive detector was used to record the SAXS patterns. The zero pixel was calibrated using a duck tendon, and the scattering vector $q$ ($q = 4\pi \sin\theta/\lambda$, where $\lambda$ is the wavelength of synchrotron X-ray beam and $\theta$ is the scattering angle) was determined by silver behenate. Measurements were carried out on a customized two-chamber hot stage at different temperatures, which were controlled to be within ±0.5 °C.

Although $G_2NB$ had a relatively low molecular weight (4530 g/mol), fibers could still be drawn in the N phase at 65 °C with a drawing ratio between 2 and 5. Typical diameter of the fibers were 20−40 $\mu$m. The temperature window of the fiber formation was, however, narrow (~10 °C). An annealing process was conducted on the fibers at 50 °C in a fixed length mode for a prolonged time (2 days). They were subsequently quenched to the room temperature for phase structure determination. 2D WAXD fiber patterns were obtained from a Rigaku automated X-ray imaging system (3000 × 3000 pixel resolution) with an 18 kW rotating anode X-ray generator. Air scattering was subtracted from the sample patterns. A hot stage was also coupled with the diffractometer to study the phase transitions at different temperatures with a heating rate of 1 °C/min.

Polarized light microscopy (PLM) experiments were performed on an Olympus HB-2 PLM coupled with a Mettler FP-90 hot stage to examine the phase morphology and LC defects. The hot-stage temperature was calibrated with standard materials. Film samples can be prepared by pressing small amounts of samples between a glass slide and a cover glass in the isotropic melt (I). The film thickness was ~10 $\mu$m. Mechanical shear was also applied on the film samples to identify the low ordered LC phase. Transmission electron microscopy (TEM, JEOL 1200 EX II) was used to observe the morphology and provide structural information. An accelerating voltage of 120 kV was used. $G_2NB$ samples were first dissolved in $CH_2Cl_2$ with 0.01% concentration and then cast onto a carbon-coated cover glass. The thickness of resulting film was less than 30 nm. These films were subsequently annealed at selected temperatures and times in order to grow larger single domains. They were shadowed with carbon and followed by platinum (Pt) at an oblique angle of 30° with respect to the sample surface. Hydrofluoric acid then was used to dissolve the cover glass and subsequently washed out by floating the samples on the surface of the distilled water, and they were picked up by Cu grids. Calibration of $d$ spacing values in the electron diffraction (ED) in TEM experiments was carried out using TlCl for $d$ spacing values smaller than 0.384 nm.

## Results and Discussion

**Thermal Phase Transition Behaviors.** Figure 1 shows two sets of DSC cooling and subsequent heating thermal diagrams of $G_2NB$ at different rates from 1 to 40 °C/min. In the entire cooling temperature range between 120 and 15 °C, one exothermic peak at a high temperature can be found. Both the onset transition temperature $T_1$ (92 °C) and the heat of transition (1.6 J/g) of this exothermic process are almost cooling rate independent although the peak width is gradually broadened with increasing cooling rates. In the low-temperature region, two overlapped exothermic processes (the higher temperature is $T_2$ having an onset temperature of 55.5 °C and the lower temperature is $T_3$) are observed at cooling rates which are slower than 10 °C/min. The $T_2$ transition is most clearly observed at a cooling rate of 2.5 °C/min in this figure. When the cooling rate is at 1 °C/min, two transitions are merged. With increasing the cooling rate, two transitions start to partially separate, and the contribution of the heat of formation of the $T_2$ phase gradually decreases. Therefore, one may expect that the $T_2$ phase formation is more cooling rate dependent compared with the $T_3$ phase formation. The overall heat of transitions (including both the $T_2$ and $T_3$ transitions) decreases with increasing cooling rate from 3.64 J/g at a rate of 1 °C/min to 2.33 J/g at a rate of 40 °C/min. Note that these two transitions are close to the $T_g$ of $G_2NB$ at 28 °C. Therefore, it is expected that when the sample was quenched to below its $T_g$, only the $T_3$ phase can be observed. This is exactly observed in our WAXD experiments (see below).

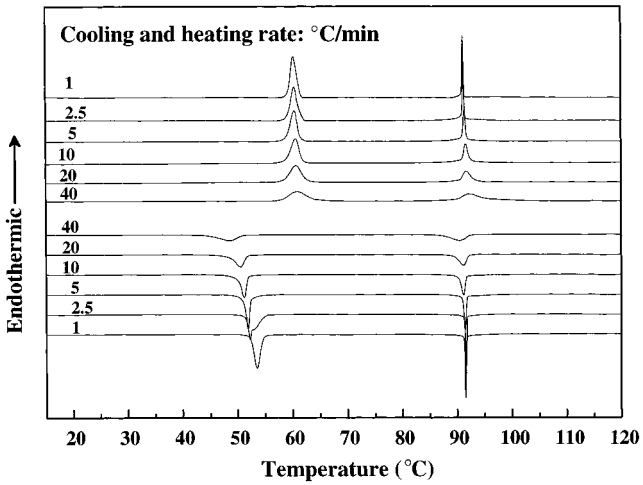


**Figure 1.** Two sets of DSC cooling and subsequent heating thermal diagrams of $G_2NB$ at different rates between 1 and 40 °C/min.

During heating, as demonstrated in Figure 1, the transition temperature $T_1$ at a high temperature of 92 °C. This corresponds to the transition observed at 92 °C during cooling. The heat of transition is also identical to that measured during cooling. On the other hand, the apparent endothermic peak at ~61 °C is relatively broad. The shape of this endothermic process also hints that more than one transition processes may be involved. The transition temperature (at ~61 °C) indicates that the structural formation needs several degree of undercooling, judged by a comparison with the DSC cooling diagrams. This undecooling is probably due to the fact that both the $T_2$ and $T_3$ transition temperatures are close to the $T_g$. The overall heat of transitions is 3.65 J/g at a heating rate of 1 °C/min, and it decreases to 2.35 J/g at 40 °C/min, which correspond well with the cooling experimental data.

Although DSC experiments provide information about the transition temperatures, the heats of transitions, and preliminary criteria to distinguish a low-ordered from a high-ordered LC phases, they cannot give rise to structural identifications of different phases. Therefore, structure-sensitive experiments, such as WAXD and ED in TEM, are necessary to be utilized.

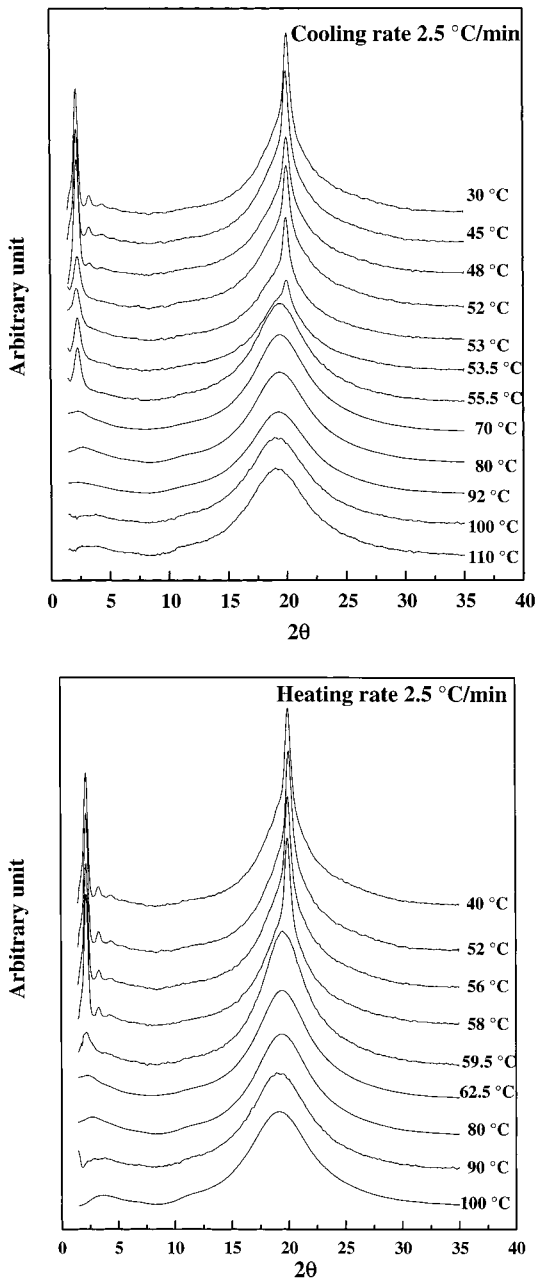


**Figure 2.** Two sets of WAXD cooling and subsequent heating thermal diagrams of $G_2NB$ at a rate of 2.5 °C/min.

**Phase Structural Changes.** Figure 2a,b shows two sets of 1D WAXD powder patterns for the $G_2NB$ at different temperatures upon cooling and heating at a rate of 2.5 °C/min. In Figure 2a, during cooling from 110 to 70 °C, no Bragg reflections can be found over the $2\theta$ range between 1.5° and 35°. Note that the high-temperature $T_1$ phase transition at 92 °C observed in DSC cooling experiments does not apparently cause any drastic WAXD pattern changes. It is speculated that this $T_1$ high-temperature transition may represent an I ↔ N phase transition. However, further experimental evidence is necessary (see below).

Continuously decreasing the temperature to 55.5 °C, a sharp Bragg reflection at $2\theta = 1.9°$ in the low $2\theta$ angle region is observed, which corresponds to the low-temperature exothermic transition of the $T_2$ phase formation observed in the DSC cooling experiment at 2.5 °C/min. No Bragg reflection in the high $2\theta$ angle region is found at this temperature. To make sure whether Bragg reflections can be observed at even lower $2\theta$ angles, 1D synchrotron SAXS experiments at different temperatures were also conducted and are shown in Figure 3. It is indeed found that this low $2\theta$ angle at 1.9° observed in the WAXD experiments is the second-order reflection, whereas the first-order reflection can be seen at $2\theta = 0.95°$, revealing a characteristic of a layered structure. This is thus a typical pattern for a smectic A or C ($S_A$ or $S_C$) phase. Further decreasing the temperature to 53.5 °C, which corresponds to the transition temperature of the $T_3$ phase in the DSC cooling experiment at 2.5 °C/min, an additional sharp Bragg reflection can be observed at $2\theta \cong 20°$. This may indicate the existence of an ordered lateral interchain packing in $G_2NB$. When the temperature further decreases, the third- and fourth-order reflections of $2\theta = 0.95°$ can also be observed (see Figures 2a,b and 3). Combining with the reflection observed at $2\theta \cong 20°$, one can conclude that the transition at $T_3$ is associated with a highly ordered LC phase formation.

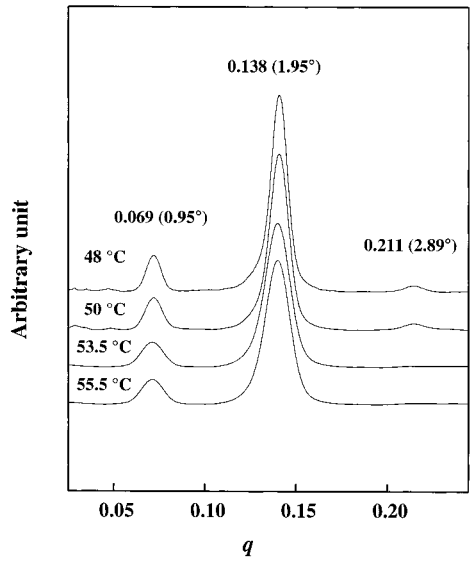


**Figure 3.** One-dimensional SAXS pattern of $G_2NB$ at different temperatures.

If the cooling rates of 1D WAXD experiments are increased, the transition temperatures of $T_2$ and $T_3$ observed in the WAXD experiments at a cooling rate of 2.5 °C/min becomes increasingly merged. Finally, at a cooling rate of 10 °C/min, the WAXD results only show that the $T_1 \rightarrow T_3$ while the $T_1 \rightarrow T_2$ transition is not experimentally assessable. This can also be proven by quenching the $G_2NB$ sample to below its $T_g$ and the WAXD pattern shows that the $T_3$ phase formation takes place. The $T_3$ phase formation cannot thus be bypassed during quenching.

Upon heating at 2.5 °C/min as shown in Figure 2b, the $T_3$ phase structure at low temperatures is retained until 58 °C. Above that temperature, the sharp Bragg reflection at $2\theta \cong 20°$ disappears. However, the low $2\theta$ angle reflections still remain up to at least close to 59.5 °C. These results indicate that there are two phase transitions overlapped in this temperature region, which are comparable with the observations in the DSC heating experiments (Figure 1). Above 59.5 °C, the low ordered S LC phase melts, and the 1D WAXD pattern

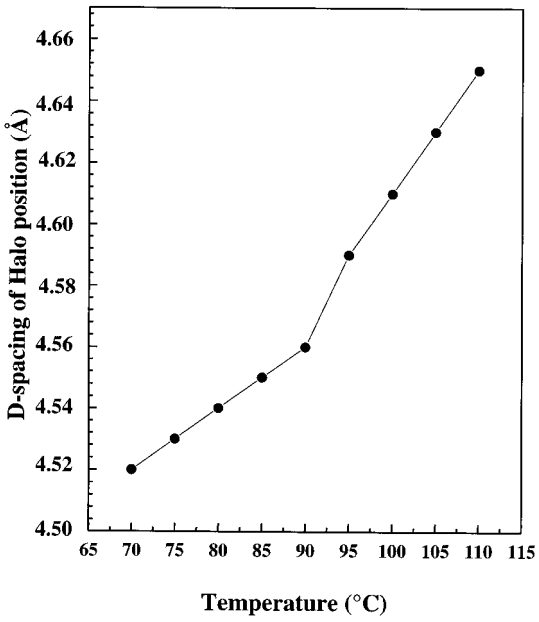


**Figure 4.** Relationship between the change of *d* spacing of the scattering halo at ~20° and temperatures.

returns to the N phase with Bragg featureless scattering in the entire $2\theta$ region studied. The detailed structures of the low-temperature $T_2$ and $T_3$ phases cannot be, however, determined on the basis of only the 1D WAXD and SAXS experiments since they do not provide structural dimensionality.

**Identification of the N Phase.** The N phase is the least ordered phase among all of the LC phases. Because the N phase transition is close to a thermodynamic equilibrium, its transition temperature and heat of transition do not usually possess a cooling rate dependence as shown in the DSC measurements (Figure 1). The 1D WAXD powder experiments in Figure 2a,b show that no Bragg reflections can be found in the entire $2\theta$ region between 1.5° and 35°, while a sudden change of the *d* spacing of the scattering halo ($2\theta \cong 20°$) at 92 °C can be recognized (Figure 4). In general, the diffuse scattering halo at $2\theta \cong 20°$ is characteristic of an average lateral distance between chains. This *d* spacing sudden change has been reported to be a representative of the transition between the I and N phases in several LC polymers.[23−28] Therefore, the structural change which corresponds to the transition at $T_1 = 92$ °C can be identified as the I ↔ N phase transition.

Further evidence for the existence of this N phase is obtained in PLM experiments as shown in Figure 5a−c. After the $G_2$NB sample is cooled through the isotropization temperature $T_1$, it becomes immediately birefringent. Figure 5a shows a fine, grainy texture observed at 90 °C, which is 2 deg below the $T_1$. After isothermally annealing the sample at this temperature for 2 h, a typical schlieren texture is observed under crossed polarizers (Figure 5b). This schlieren texture displays dark brushes emanated by singularities. The point singularities of both two and four brushes can be found in Figure 5b, indicating that this LC phase is a N phase.

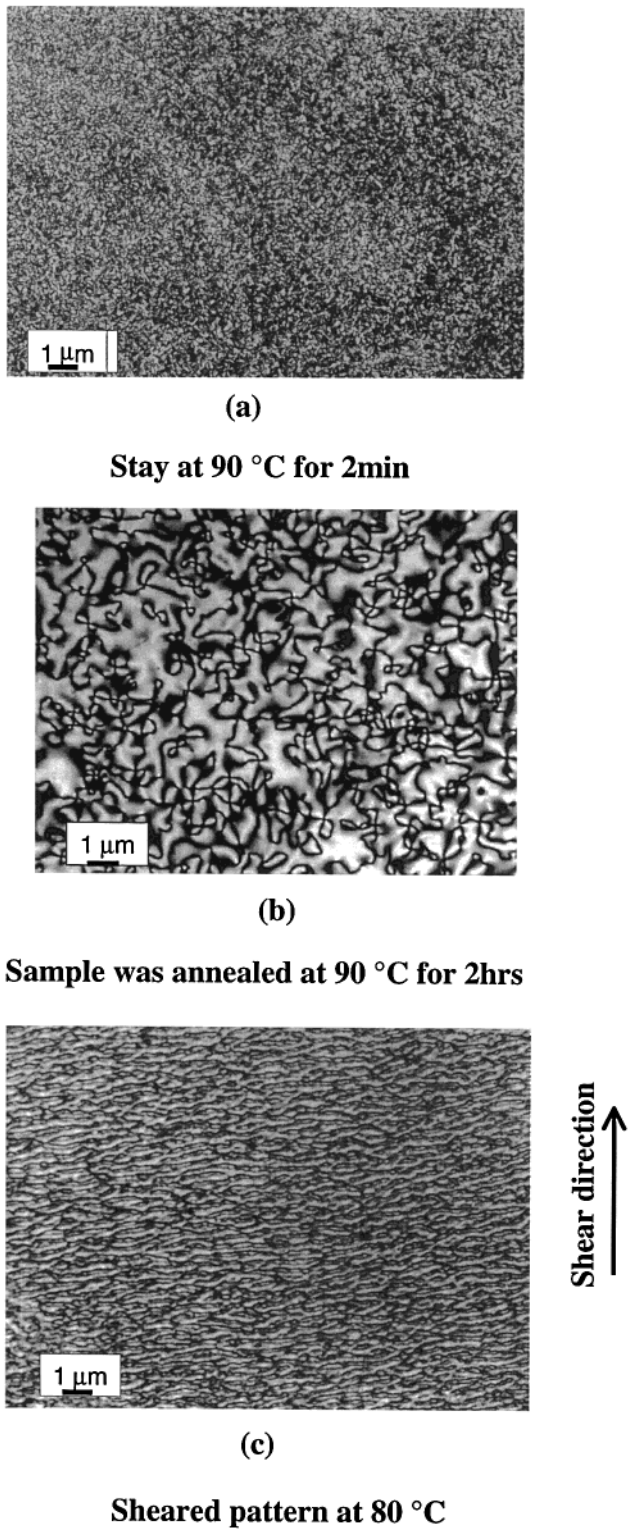


**Figure 5.** PLM microphotographs of G2NB at 90 °C for 2 min (a), at 90 °C for 2 h (b), and mechanically sheared at 80 °C (c).

(23) Ungar, G.; Feijoo, J. L.; Percec, V.; Tound, R. *Macromolecules* **1991**, *24*, 953.
(24) Yandrisits, M. A.; Cheng, S. Z. D.; Zhang, A.-Q.; Cheng, J.; Wunderlich, B.; Percec, V. *Macromolecules* **1992**, *25*, 2112.
(25) Pardey, R.; Zhang, A.; Gabori, P. A.; Harris, F. W.; Cheng, S. Z. D.; Adduci, J.; Facinelli, J. V.; Lenz, R. W. *Macromolecules* **1992**, *25*, 5060.
(26) Pardey, P.; Shen, D.; Gabori, P. A.; Harris, F. W.; Cheng, S. Z. D.; Adduci, J.; Facinelli, J. V.; Lenz, R. W. *Macromolecules* **1993**, *26*, 3687.
(27) Yoon, Y.; Zhang, A.; Ho, R.-M.; Cheng, S. Z. D.; Percec, V.; Chu, P. *Macromolecules* **1996**, *29*, 294.
(28) Yoon, Y.; Ho, R.-M.; Moon, B.-S.; Kim, D.; McCreight, K. W.; Li, F.; Harris, F. W.; Cheng, S. Z. D.; Percec, V.; Chu, P. *Macromolecules* **1996**, *29*, 3421.

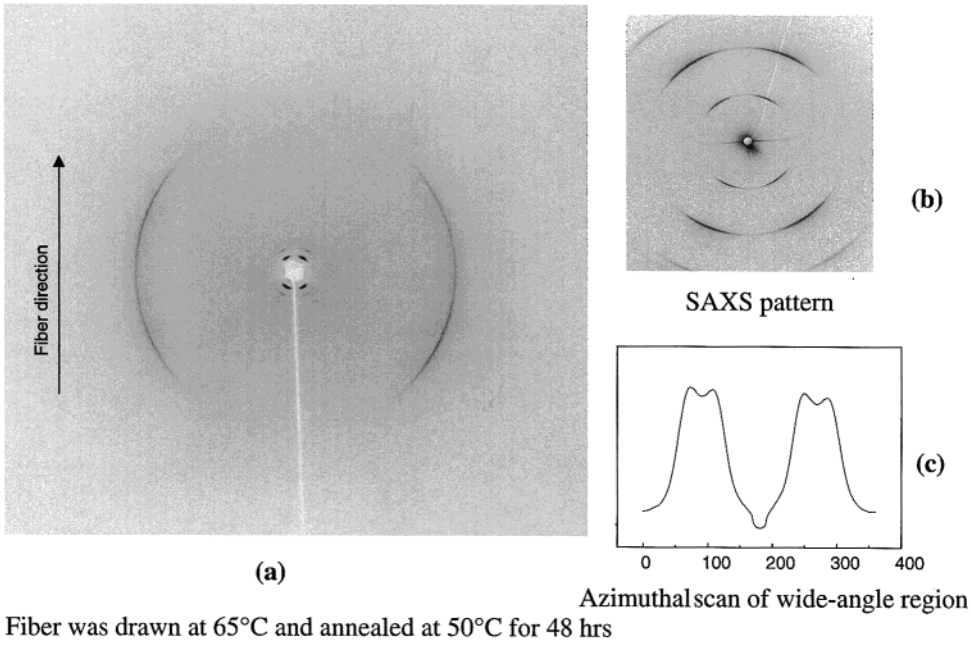


**Figure 6.** 2D fiber patterns of $G_2NB$ after annealing for 2 days at 50 °C in the WAXD region (a), in the SAXS region (b), and an azimuthal scan of the WAXD region (c).

Figure 5c shows the $G_2NB$ morphology of this N phase in PLM after an external mechanical shear at 80 °C between two cover-glass slides and slightly annealed at this temperature. The banded texture with a spacing of 0.5−1 $\mu$m is seen which is perpendicular to the shearing direction. This type of share-induced banded textures is viewed as a typical orientationally ordered pattern of main-chain LC polymers in a low ordered LC phase.[24−28] It is interesting that in $G_2NB$, which possesses a molecular weight of 4530 g/mol and multiple branches, the banded texture can also be observed although these bands are not as regular as those observed in the main-chain LC polymers.

**Identification of the Low-Temperature $T_3$ LC Phase.** $G_2NB$ exhibits the structural change in the low-temperature region between 45 and 60 °C, documented by the 1D WAXD patterns as shown in Figure 2a,b. To identify these ordered structures, we need to have 2D WAXD fiber patterns. In Figure 6a, two sets of the "X" reflections in the fiber pattern can be observed. The first "X" set is located in the quadrants of the low $2\theta$ angle region (see Figure 6b), which shows at least up to third-order reflection. Ratios of the scattering vectors $q$ ($q = 4\pi \sin \theta/\lambda$) values of these low angle reflections are 1:2:3, indicating the existence of a layered structure. The layer normal is tilted with respect to the fiber axis. The layer $d$ spacing can be calculated from the first-order reflection, and it is 9.06 nm. It is surprising that the intensity of the second-order reflection is stronger than that of the first-order reflection (see below). Another "X" set of reflections is in the quadrants at $2\theta \cong 20°$, which correspond to a $d$ spacing of ∼0.45 nm. This indicates that a highly ordered lateral hexagonal packing among the chains (specifically, mesogens) exists in this LC phase, the chain direction, and thus, the mesogenic orientation direction is tilted with respect to the fiber axis. In the azimuthal scan, those four arcs at $2\theta \cong 20°$are clearly identified as shown in Figure 6c.

An interesting observation in this fiber pattern is when the fiber is drawn in different drawing ratios, both the tilt angles of the layer normal and mesogenic orientation direction with respect to the fiber axis change. Tilt angles of the layer normal are observed to vary in a wide range from 15° to 65°. Even when a fiber with a fixed drawing ratio but being annealed at different temperatures and/or times, both the tilt angles of the layer normal and the mesogenic orientation direction can change. However, no matter how the tilt angles of the layer normal and the mesogenic orientation direction change with respect to the fiber axis, the interrelationship between these two tilt angles is invariant. As shown in Figure 7, when two dashed lines are drawn across both "X" sets of reflection maxima diagonally along the opposite directions in the low and high $2\theta$ angle regions, the angle between these two lines is always 90°. This indicates that although both the layer

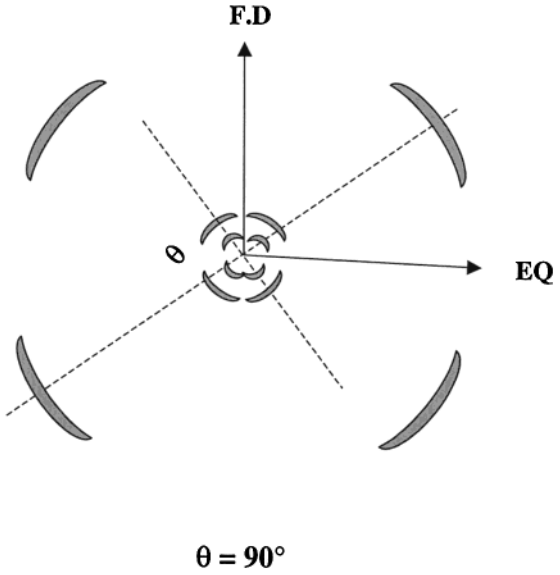


**Figure 7.** Schematic of a 2D $G_2NB$ fiber pattern to illustrate the interrelation between the low-angle and high-angle "X" shaped reflections.

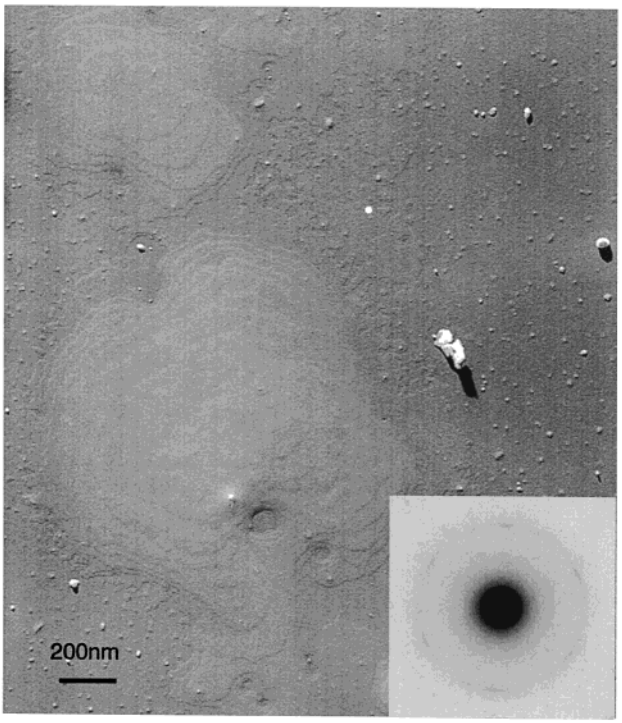


**Figure 8.** Flat lamellar morphology in TEM and the ED of $G_2NB$ for the low-temperature $T_3$ phase.

normal and the mesogenic orientation direction are tilted with respect to the fiber direction, the long axis of the mesogens within the layer is always parallel to the layer normal. A possible explanation for this observation is due to the cooperative mobility of the supramolecular layer structure of the low molecular weight $G_2NB$ monodendrons with the molecular mesogens, similar to the observation recently reported.[29,30]

Detailed structural information about the lateral packing within the layers can also be obtained using ED experiments in TEM. The sample was prepared from diluted solution and annealed at 50 °C for 4 days in order to develop the $T_3$ phase. Figure 8 shows the flat-on lamellar morphology, and the ED pattern is included in this figure. A hexagonal lattice with six arcs can be observed, and the *d* spacing is 0.45 nm. This indicates that the mesogens are perpendicular to the substrate and packed into a 6-fold hexagonal array. Since the intensity of these six arcs are weak and no higher ordered reflections are observed, it seems that no long-range atomic positional order exists in this hexagonal array within the layers. Combining the results of the 1D and 2D WAXD and the ED observations, a hexatic B ($S_h^B$) highly ordered LC phase can be identified.[31,32] Note that this $S_h^B$ phase identification in $G_2NB$ is on the basis of the definition from the low molecular weight liquid crystals of which only the interrelationship between the layer normal and the mesogen orientation direction is taken into account.

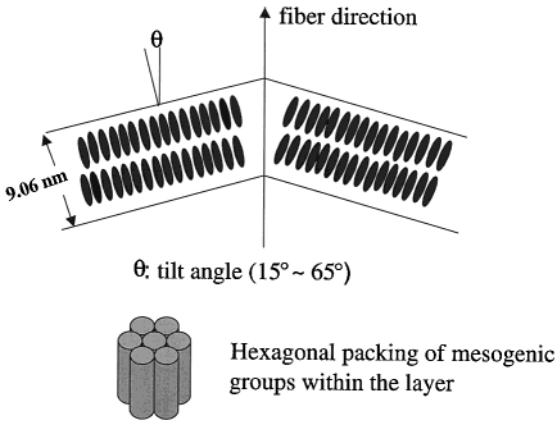


**Figure 9.** Schematic of layered structure and lateral packing of the mesogens within the layers in the $S_h^B$ phase.

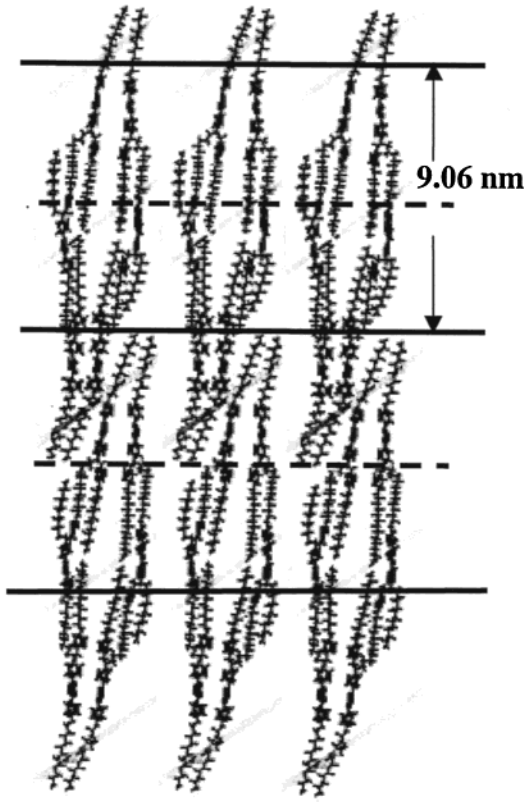


**Figure 10.** Possible molecular packing model of the $S_h^B$ phase.[16]

Usually, the layer *d* spacing in a S phase of a main-chain LC polymer represents a length of chemical repeat unit which consists of one mesogen and spacers such as methylene units. However, in this case, the layer *d* spacing is 9.06 nm, which is many times larger than the length of the chemical repeat unit. In fact, the layer structure in this $S_h^B$ phase of $G_2NB$ is constructed by the monodendrons themselves. Figure 9 provides a 2D schematic illustration of the layered structure and the packing of the mesogens (solid elongated shapes) within the layers. The $\theta$ angle stands for the tilt angle of layer normal with respect to the fiber axis. The lateral hexagonal packing of the mesogens within the layered structure is also given in this figure.

Figure 10 presents a possible molecular arrangement within the layered structure in the $S_h^B$ phase. The

(29) Leland, M.; Wu, Z.; Chhajer, M.; Ho, R.-M.; Cheng, S. Z. D.; Keller, A.; Kricheldorf, H. R. *Macromolecules* **1997**, *30*, 5249.
(30) Leland, M.; Wu, Z.; Ho, R.-M.; Cheng, S. Z. D.; Kricheldorf, H. R. *Macromolecules* **1998**, *31*, 22.
(31) Gray, G. W.; Goodby, J. W. G. *Smectic Liquid Crystals: Textures and Structures*; Leonard Hill: London, 1984.
(32) Pershan, P. S. *Structure of Liquid Crystal Phases*; World Scientific: Singapore, 1988.

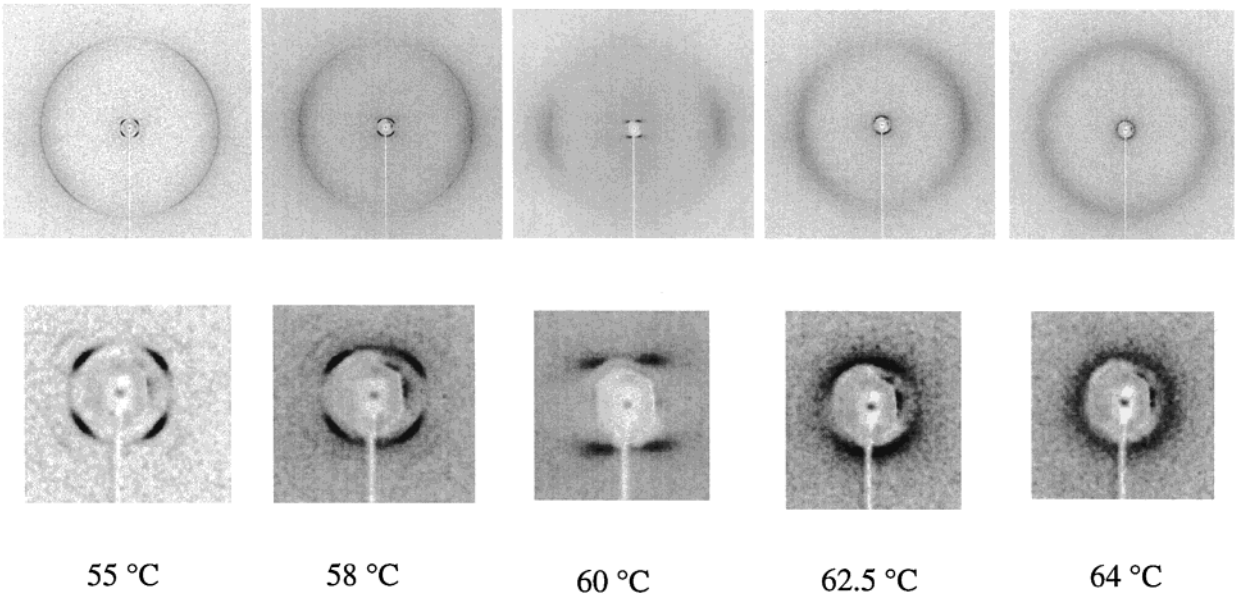


**Figure 11.** 2D WAXD and SAXS fiber patterns of the $G_2NB$ during heating at 55 (a), 58 (b), 60 (c), 62.5 (d), and 64 °C (e).

lateral order is not meant to represent true molecular translational periodicity. This model is constructed on the basis of computer simulations of the second generation $G_2NB$ LC monodendrons previously published.[16] The monodendrons adopt the anti conformation when they are packed in the layered structure. In this model, the chain ends are accumulated not only at the layer boundaries but at the center of the layers (dashed lines in Figure 10), which results in an additional electron density difference at the halfway across the layer profile. This generates a partial extinction of the first-order reflection to cause the intensity of second-order reflection to be stronger than that of the first-order reflection in the low $2\theta$ angle region.

**Identification of the Intermediate-Temperature $T_2$ LC Phase.** From the DSC results in Figure 1, the $T_2$ phase formation at 55.5 °C, while in the 1D WAXD experiments shown in Figure 2a, a sharp diffraction peak with $S_h^B$ is observed at and below 55.5 °C during cooling, which is the second-order reflection of the layer structure. No Bragg reflection is found in the high $2\theta$ angle region at this temperature. Although in Figure 6 it is shown that the layer normal is tilted with respect to the fiber axis, this is not sufficient to conclude that this is a $S_C$ phase since in a $S_C$ phase, the average mesgonic orientation direction must be tilted with respect to the later normal.

Because the temperature region for this S phase is narrow (~2 °C), a nonisothermal 2D WAXD experiment was carried out at a heating rate of 1 °C/min from 55 to 64 °C, and the results are shown in Figure 11a−e. At 55 °C, the $S_h^B$ phase is observed (Figure 11a). When the temperature is increased to 60 °C as shown in Figure 11c, the ordered lateral hexagonal packing, which is represented by the sharp reflections at $2\theta \cong 20°$ in the quadrants disappear first, and a pair of diffuse scattering halos in the high $2\theta$ angle region are observed along the equator. The diffraction peaks in the low $2\theta$ angle region change their shapes and become diffuse compared with Figure 11a,b, but they remain in their positions in the quadrants. Therefore, Figure 11c represents a $S_C$ LC phase in the narrow temperature region of ~2 °C due to the fact that the mesogenic orientation direction is tilted with respect to the layer normal. Further increasing temperature to 64 °C (Figure 11e), all the lateral packing orientation is lost, and the layer reflections are significantly diffuse, indicating an entrance of the N phase.

However, there is another issue that needs to be further discussed. Namely, the development of the $S_C$ phase (the $T_2$ phase formation) is more cooling rate dependent than that of the $S_h^B$ phase (the $T_3$ phase formation). Adjusting the cooling rate, the $S_C$ phase can be observed at slow cooling rates and hidden at fast cooling rates in which this $S_C$ phase becomes metastable.[33,34] This may be due to the fact that the $S_C$ phase is constructed by the supramolecular layer structure, while the $S_h^B$ phase is formed by combining both the supramolecular layer structure and the molecular lateral hexagonal packing. It has been found that the formation of a supramolecular LC structure shows stronger cooling rate dependent compared with that of the molecular LC structure due to molecular cooperative dynamics.[35] Therefore, it is conceivable that the supramolecular layer structure formation in the $S_C$ phase requires the stronger cooling rate dependence, while the $S_h^B$ phase is induced by the self-assembled mesogins to induce the supramolecular layer structure, and consequently, the $S_h^B$ phase needs less cooling rate dependence. During heating, the molecular lateral hexagonal packing melts first at 58 °C, and the supramolecular layer structure stays on until above 59.5 °C since the layer structure cannot be diminished before the molecular packing is released.

## Conclusion

In summary, phase transitions and their structures of the second generation monodendron $G_2NB$ based on

(33) Keller, A.; Cheng, S. Z. D. *Polymer* **1998**, *39*, 4461.
(34) Cheng, S. Z. D.; Keller, A. *Annu. Rev. Mater. Sci.* **1998**, *28*, 533.
(35) Tu, H.; Wan, X.; Liu, Y.; Chen, X.; Zhang, D.; Zhou, Q.-F.; Ge, J. J.; 36. Shen, Z.; Jin, S.; Cheng, S. Z. D. *Macromolecules* **2000**, *33*, 6315.

the $AB_2$ mesogenic monomer, 13-hydroxy-1-(4-hydroxyphenyl)-2-(4-hydroxy-4″-*p*-terphenylyl)tridecane, are identified using combined characterization techniques. DSC, 1D WAXD, and SAXS powder experiments show that this $G_2$NB monodendron exhibits multiple LC phases. 2D WAXD, SAXS, and ED experiments identify these phase structures. The equilibrium phase transition sequence is $S_h^B \leftrightarrow S_C \leftrightarrow N \leftrightarrow I$. It is interesting that although the layer normal in the $S_h^B$ phase is tilted with respect to the fiber axis, the mesogenic orientation direction within the layer is always parallel to the layer normal, and their lateral packing forms a hexagonal array. In the $S_C$ phase, on the other hand, the chain direction is parallel to the fiber axis and tilted with respect to the layer normal. Only liquidlike short-range order exists within the layers. Furthermore, the layer spacing of these $S_h^B$ and $S_C$ phases are much larger than the chemical repeat unit of the LC monomer; rather, it is a representative of the whole size of the $G_2$NB monodendron as a supramolecular structure. This may be responsible for the stronger cooling rate dependence of the formation of the supramolecular layer structure in the $S_C$ phase compared with that of the $S_h^B$ phase.

**Acknowledgment.** This work was supported by the National Science Foundation (DMR-9617030) and the Science and Technology Center for Advanced Liquid Crystal Optical Materials (ALCOM) at Kent State University, Case Western Reserve University, and the University of Akron (DMR-9157738).

CM0117228